Electric Stress Analysis of Non-Uniform Hydrophobic Surface of 400 KV High Voltage Polymer Insulator

Vrushank S. Chavan

The Maharaja Sayajirao University of Baroda, India
Email: *vrushank.msu[at]gmail.com*

Abstract: ***Polymer insulators are widely used in HV transmission due to their intrinsic hydrophobicity, which prevents water film formation and leakage current. However, hydrophobicity degrades non-uniformly in service, typically weakening near the end fittings, yet most studies assume uniform surface behavior. This study numerically investigates electric field and potential distribution along a 400 kV alternating shed polymer insulator under non-uniform hydrophobicity using COMSOL Multiphysics. Three hydrophilic fractions (22.2%, 66.7%, 100%) were modeled alongside a clean and dry condition, using Hydrophobicity Class 7 and Class 2 to represent the hydrophobic and hydrophilic regions. Results show the peak field does not vary monotonically with hydrophilic fraction, 22.2% produced the highest stress, nearly five times the dry condition, due to conductivity discontinuity at the wet-dry boundary, while higher fractions showed fields comparable to or below the dry case. Terminal current increased only marginally with hydrophilic fraction, uncorrelated with the local field enhancement, indicating that partial hydrophobicity loss poses greater flashover risk than complete loss, and that leakage current monitoring alone is insufficient for its detection.***

Keywords: Electric stress, Hydrophobicity, Polymer Insulator, Leakage Current

1. Introduction

Polymer insulators, commercially introduced in the 1970s, emerged as a lighter and more flexible alternative to traditional porcelain insulators, consisting of a fiber reinforced plastic (FRP) core for mechanical strength, a silicone rubber or EPDM housing for electrical insulation, and metal end fittings for line connection. Their adoption was driven largely by the limitations of porcelain insulators, namely, considerable weight, hydrophilic surface behavior, susceptibility to pollution-induced flashover, and intensive maintenance requirements in coastal and industrially polluted environments. In comparison, polymer insulators offer intrinsic hydrophobicity that inhibits continuous water film formation and reduces leakage current, along with a unique self-recovery mechanism wherein low molecular weight silicone migrates to the surface to restore hydrophobicity after contamination or discharge activity, a property porcelain fundamentally lacks [1],[2]. Additionally, polymer insulators exhibit a superior strength-to-weight ratio, greater resistance to vandalism and brittle fracture, lower maintenance demands, and improved flashover performance under wet and polluted conditions, making them increasingly preferred for modern high voltage transmission networks [3]. Performance of polymer insulators depends on surface hydrophobicity which can degrade over time, Hydrophobicity degradation can result from several factors, including corona discharge [4],[5]. arc discharge [6], prolonged exposure to extreme wetting conditions [7], ultraviolet radiation [8], and the accumulation of surface contaminants [9]. The electric field along a string is known to be nonuniform, it is strongest at the high voltage end, next strongest at the grounded end, and weakest in the middle, this has been confirmed by both simulations and experimental measurements [10],[11]. Since discharge occurs preferentially where the field is strongest, breakdown is more likely to occur at the high-voltage and ground ends than in the middle [12]. There are various studies carried out to analyze the insulator performance under wet conditions, wetting intensifies the electric field at shed edges and terminals, with the alternating shed insulator experiencing higher field stress than the constant-shed design due to its larger shed diameter and longer creepage distance [13]. Uniform pollution smooths the voltage distribution and reduces overall field stress, whereas non-uniform pollution and water droplets each independently and jointly intensify local field concentrations [14]. Under clean and dry and uniformly polluted conditions, the electric field remains low and largely unchanged, with end fittings being the most stressed region. Non-uniform pollution conductivity further shortens the effective leakage distance by shifting the effective grounding point toward the lower conductivity region, increasing the likelihood of flashover [15]. Under severely degraded hydrophobicity, the field aged composite insulator exhibited a maximum electric field intensity approximately 12 times greater than that of the pristine insulator, with intensification predominantly localized at the shed surfaces and shank regions surpassing the corona inception threshold at these locations [16]. Moreover, Non-uniform hydrophobicity distribution causes a nonmonotonic flashover voltage trend, with certain partial hydrophobic configurations performing worse than a fully hydrophilic insulator. This occurs because the wetted hydrophilic region forces voltage onto the remaining hydrophobic section, concentrating electric field stress [17].

Previous studies have analyzed critical stress characteristics under uniform and nonuniform pollution and wetting

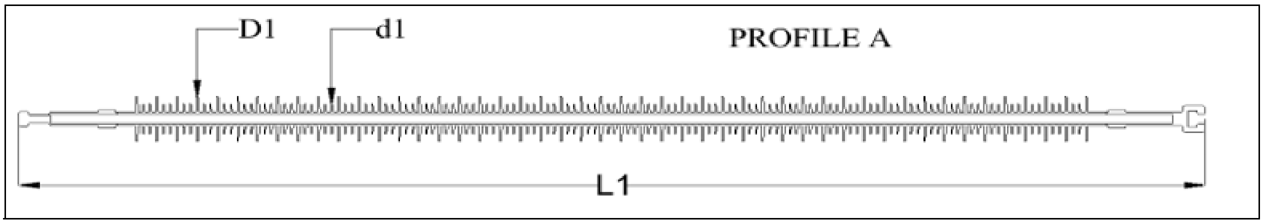

(a)

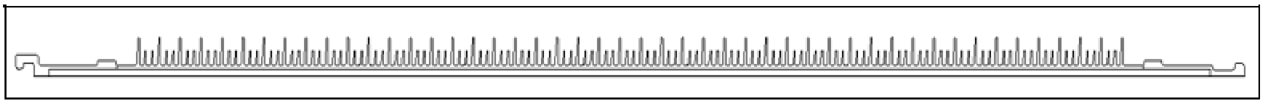

(b)

Figure 1: 2D Polymer Insulator Models, where (a) 400 KV Polymer Insulator Model, (b) Axisymmetric Model

conditions, and considered uniform hydrophobicity across the insulator surface. In practice, however, hydrophobicity loss is non-uniform. It is therefore necessary to analyze insulator performance under non-uniform surface hydrophobicity conditions to accurately evaluate their critical stress characteristics.

2. Insulator Model and Numerical Analysis

2.1 Insulator Modelling

As shown in figure 1 (a), the insulator studied Profile A is rated for 400 kV and has an overall length L1 of 2700 mm. It uses an alternating shed design, with large sheds of diameter D1 is120 mm and small sheds of diameter d1 is 80 mm. There are 48 large sheds N1 and 94 small sheds n1, making a total of 142 sheds T1 along the insulator, given in table 1[18]. This alternating shed pattern helps increase the leakage distance and improves the insulator's performance under polluted or wet conditions. Figure 1 (b) shows the axis symmetric model of the insulator which is used in simulation.

Table 1: Technical Specifications [18]

Parameter	*Symbol*	*Profile A*
Voltage Ratings	Volts	400KV
Overall insulator length	L1	2700 mm
Large shed diameter	D1	120 mm
Small shed diameter	d1	80 mm
No. of large sheds	N1	48
No. of small sheds	n1	94
Total sheds	T1	142

2.2 Hydrophobicity Modelling

A common characteristic observed during service is the reduction of hydrophobicity toward the two ends of an insulator. To represent different patterns of hydrophobicity along the insulator, this variation can be modeled by adjusting the number of hydrophobic units considered. This is captured through the hydrophilic fraction, p, defined as the ratio of the hydrophilic section's dry arcing distance to the total dry arcing distance of the insulator[17] , as shown in Equation (1):

$$p = H_{hydrophilic} / H \quad (1)$$

Here, p denotes the hydrophilic fraction, $H_{hydrophilic}$ represents the dry arcing distance of the hydrophilic portion, and H is the overall dry arcing distance of the insulator. For our simulation we had considered p values as 22.2 %, 66.7 % and 100 %. In this study, Hydrophobicity Class 7 (HC 7) was considered for the hydrophilic fraction, while Hydrophobicity Class 2 (HC 2) was considered for the hydrophobic fraction. Accordingly, a uniform water layer of 0.5 mm thickness was assumed to represent the wetting condition for HC 7, whereas uniform distribution of semi-hemispherical water droplet of 2mm diameter was considered to represent the wetting condition for HC 2 [17][19], as presented in figure 2.

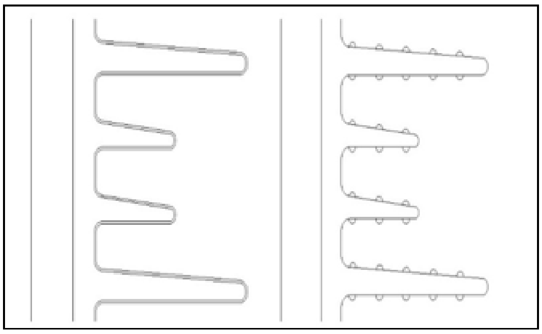

Figure 2: Hydrophilic and Hydrophobic section of the Insulator

2.3 Numerical Analysis

The electric field and current distribution along the insulator surface were simulated using the Electric Currents physics interface under Frequency Domain study, which solves for the quasi-static electromagnetic behavior of the system at the operating power frequency. This physics interface is governed by the continuity equation for current density and the constitutive relations for electric field and displacement current, expressed as in equation (2), (3) and (4).

$$\nabla \cdot J = Q\_j, v \quad (2)$$
$$J = \sigma E + j\omega D + J\_e \quad (3)$$
$$E = -\nabla V \quad (4)$$

where J is the current density, Q_j,v is the current source, σ is the electrical conductivity, ω is the angular frequency, D is the electric displacement field, J_e is an externally generated current density, E is the electric field, and V is the electric potential.

The insulator geometry, along with the assigned hydrophilic (HC 7) and hydrophobic (HC 2) regions, was modeled with their respective water film and droplet configurations to represent the surface wetting conditions. The material properties, including the conductivity of the water layer, droplets, and insulator body, were assigned accordingly as given in table 2. A voltage of 326.6 kV (peak phase voltage of the 400 kV system) was applied at the high-voltage terminal, while the ground terminal was set to zero potential, and the frequency domain study was carried out at 50 Hz to replicate realistic operating conditions. The resulting electric field and potential distribution along the insulator surface were then extracted for further analysis.

Table 2: Electrical Properties of Materials

Domain	*Material*	*εr*	*Conductivity σ S/m*
Surrounding medium	Air	1	1e-15
End fittings	Metal	1e10	5.9e7
Shed housing	SiR	4.3	1e-14
Core rod	FRP	7.2	1e-14
Water layer	water	81	6e-7
Water droplet	water	81	180e-6

3. Results and Discussion

Figure 3 shows the 2D contour plot of the electric potential distribution around the insulator under clean and dry conditions. The potential varies from a maximum of 326.599 kV at the high-voltage end to a minimum of 0 kV at the grounded end, consistent with the applied boundary conditions. The equipotential contours are closely spaced near the two terminal ends of the insulator, indicating higher voltage gradients and hence higher electric field in these regions, while the contours are widely and uniformly spaced across the surrounding air domain and along the central portion of the insulator, reflecting a more gradual potential decay. Figure 4 presents the distribution of the electric field norm along the arc length of the insulator for varying hydrophilic fractions (22.2%, 66.7%, and 100%), compared against the clean and dry reference condition. As expected, the electric field exhibits a characteristic non-uniform profile, with pronounced maxima near the two end regions of the insulator and a substantially lower, near-uniform field along the central shed region. This behavior reflects the well-known field concentration effect at the electrode ends of a string insulator.

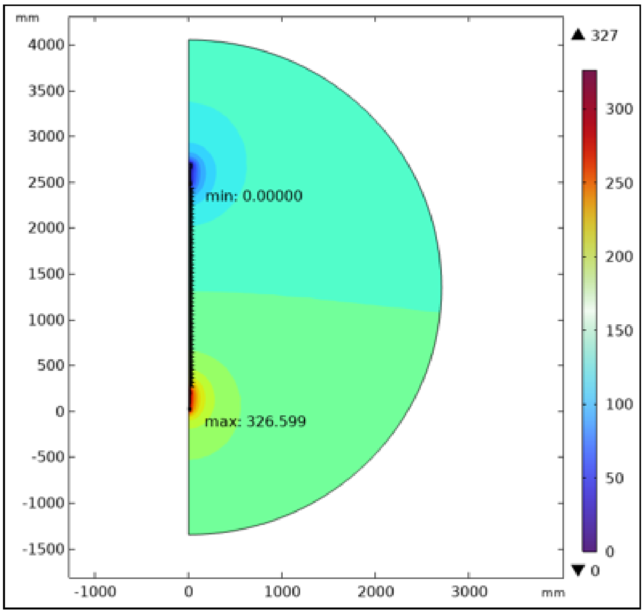

Figure 3: 2D Contour Plot of Potential Distribution under Clean and Dry Condition

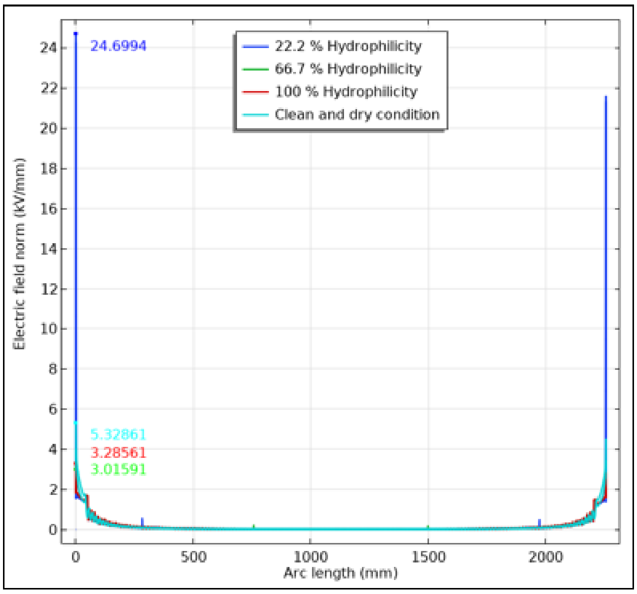

Figure 4: Electric Field Norm along the Arc Length of Insulator Under Various Hydrophobic Conditions

A notable observation is that the maximum electric field stress does not increase monotonically with hydrophilicity. The lowest hydrophilic fraction 22.2% produces the highest peak field of 24.6994 kV/mm, which is nearly five times greater than the peak field of 5.32861 kV/mm obtained for the clean and dry condition. In contrast, as the hydrophilic fraction increases to 66.7% and 100%, the peak field reduces to 3.01591 kV/mm and 3.28561 kV/mm respectively, both lower than the clean and dry case. This is attributed to the discontinuity in surface conductivity. As the hydrophilic fraction increases further and the water film becomes more continuous 66.7% and 100%, the surface behaves more like a uniformly conductive layer, allowing a more even voltage distribution and consequently a reduction in localized field stress below even the dry condition. These results suggest that a partially hydrophobic insulator surface, rather than being safer, can be more prone to localized electric field concentration than a fully wetted or completely dry insulator, which has direct implications for the risk of dry-band arcing and flashover initiation under non-uniform wetting conditions in service.

Figure 5 shows the electric potential distribution along the arc length of the insulator for different hydrophilic fractions (22.2%, 66.7%, and 100%) compared with the clean and dry condition. The potential decreases monotonically from about 326 kV at the high-voltage end to 0 kV at the grounded end, with a steep drop near both terminals and a gradual, near-linear decline across the central region, consistent with the field concentration observed near the ends in the field distribution plot.

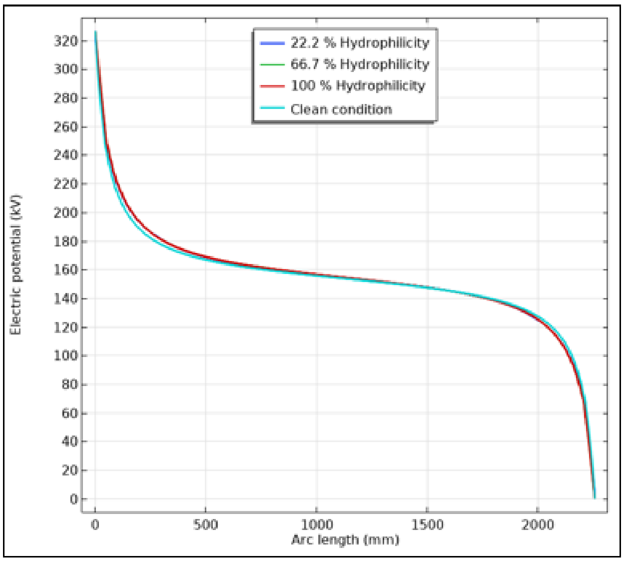

Figure 5: Electric potential distribution along the arc length of insulator under various hydrophobic conditions

Unlike the electric field results, the potential curves for all four conditions nearly overlap along the entire arc length, showing only marginal differences near the ends. This indicates that the overall voltage distribution is largely governed by the insulator's bulk geometry and boundary conditions, and is relatively insensitive to the hydrophobicity pattern, unlike the electric field, which is highly sensitive to local wet-dry surface discontinuities. This confirms that the primary concern from partial surface wetting is localized field enhancement rather than any significant change in the global voltage grading of the insulator.

Figure 6 presents the 2D electric field norm contour plots near the high-voltage (HV) end of the insulator for the clean and dry condition and the three hydrophilicity levels 22.2%, 66.7%, and 100%. The maximum field values obtained are summarized in Table 3, 9.1446 kV/mm for the clean condition, 25.846 kV/mm for 22.2% hydrophilicity, 9.0095 kV/mm for 66.7% hydrophilicity, and 9.0043 kV/mm for 100% hydrophilicity.

Table 3: Max. electric field norm under various hydrophobic conditions

Highest Electric field norm (kV/mm)	
Clean Condition	9.1446
22.2 % Hydrophilicity	25.846
66.7 % Hydrophilicity	9.0095
100 % Hydrophilicity	9.0043

The contour plots clearly show that the electric field is most intensely concentrated at the first shed near the HV end in all cases, as indicated by the tightly packed field contours in this region. For the 22.2% hydrophilicity case, the field crowding is markedly denser and more localized around the first shed tip, corresponding to the sharp field enhancement (25.846 kV/mm). This is due to sharp discontinuity in surface conductivity, leading to severe local field intensification at the wet-dry boundary.

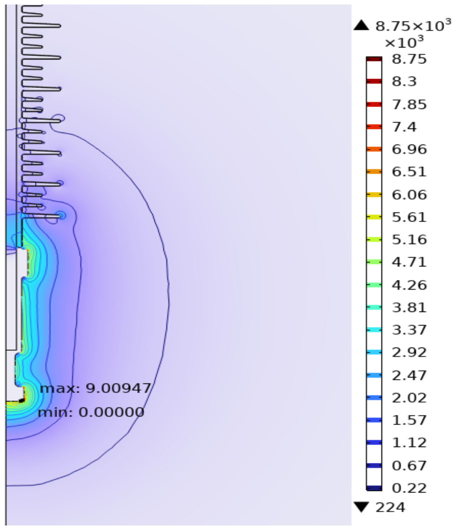

(a)

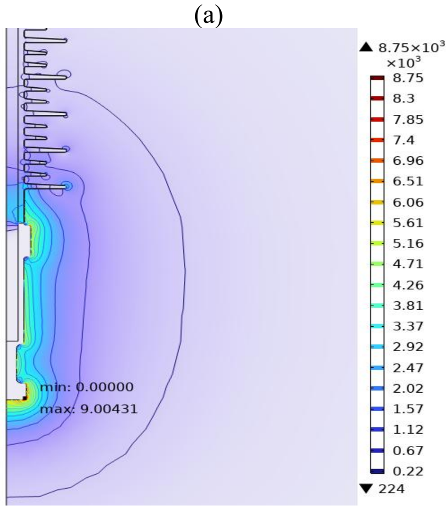

(b)

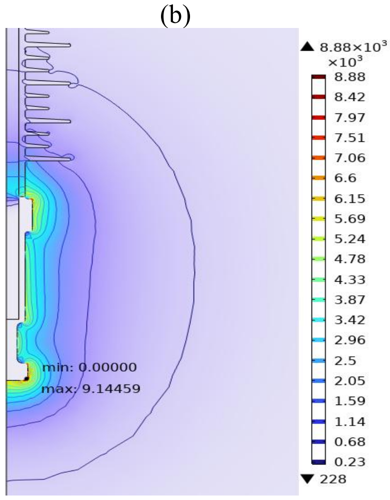

(c)

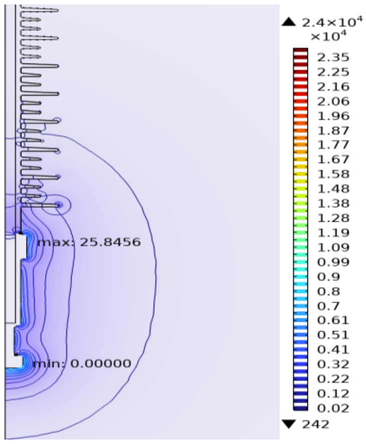

(d)

Figure 6: 2D Electric field norm contour plots near the high-voltage (HV) end of the insulator for (a) 66.7 %, (b) 100 %, (c) Clean and dry and (d) 22.2 % hydrophilic fractions.

In contrast, for the 66.7% and 100% hydrophilicity cases, the field contours are more evenly distributed over a larger surface area, resulting in lower peak field values 9.0095 kV/mm and 9.0043 kV/mm respectively, similar in magnitude to the clean and dry condition (9.1446 kV/mm). This confirms that as the hydrophilic coverage increases and the wetted film becomes more continuous, the surface behaves closer to a uniformly conductive layer, allowing the field to spread more evenly and avoiding sharp localized stress concentrations. A similar but comparatively lower field enhancement was observed at the grounded end of the insulator, as seen in the arc-length field distribution Figure 6, confirming that the HV end represents the critical region governing the insulator's overall field stress and potential risk of dry-band arcing

These results reinforce the earlier arc-length field distribution findings, visually confirming that the most critical field enhancement occurs under low hydrophilicity conditions rather than under fully wetted or fully dry surfaces, highlighting the HV end first shed as the most vulnerable location for dry band arcing initiation.

Table 4 presents the complex terminal current values obtained for the different hydrophilicity conditions, along with their resistive and capacitive components. A key observation is that the clean and dry condition exhibits a purely capacitive current with zero real component, indicating ideal dielectric behavior where the insulator behaves as a pure capacitor with negligible resistive leakage. In contrast, all wetted conditions 22.2%, 66.7%, and 100% hydrophilicity introduce a finite real component, confirming the presence of a resistive leakage current path along the wetted surface, caused by the conductive water film and droplets bridging the insulator surface.

As the hydrophilic fraction increases from 22.2% to 100%, both the real and imaginary components of the terminal current show a gradual, marginal increase (real: 25.282 to 26.860 μA, imaginary: 355.46 to 357.08 μA). This trend indicates that a larger wetted area contributes to a slightly higher overall leakage current and effective surface capacitance, as more conductive surface area is available for current flow.

Table 4: Terminal current values under various hydrophobic conditions

Hydrophilic Fraction p	*Terminal Current (μA)*
Clean and dry	336.96i
22.2 %	25.282+355.46i
66.7 %	26.841+357.07i
100 %	26.860+357.08i

These results are particularly useful when correlated with the electric field distribution findings. Although the 22.2% hydrophilicity case exhibited the most severe localized electric field enhancement i.e., 25.846 kV/mm, its terminal leakage current remains only marginally lower than the more uniformly wetted cases. This suggests that the risk associated with partial wetting is not reflected in the terminal current but rather manifests as a highly localized field concentration. In practical terms, this implies that terminal current monitoring alone may not be a reliable indicator of the localized high-field stress responsible for dry band arcing initiation, since the bulk current signature remains largely similar across wetting conditions, while the actual electrical stress and consequent risk of surface discharge activity vary significantly at the local scale.

This distinction is critical from a diagnostic and asset management perspective, it highlights those field based localized stress indicators rather than solely current based leakage monitoring, this may be necessary to accurately assess degradation risk in insulators under partial or non-uniform hydrophobicity conditions.

4. Conclusion

This study numerically investigated the electric field and potential distribution along a 400 kV alternating-shed polymer insulator under non-uniform surface hydrophobicity. Three hydrophilic fractions (22.2%, 66.7%, and 100%) were analyzed alongside a clean and dry reference condition to represent typical hydrophobicity loss near the insulator end fittings.

The results show that the electric field is highly sensitive to the spatial pattern of surface wetting, while the voltage distribution remains largely governed by the insulator's bulk geometry and is relatively insensitive to hydrophobicity condition. Notably, the peak field stress does not vary monotonically with hydrophilic fraction, the lowest fraction (22.2%) produced the highest field intensity (25.846 kV/mm at the HV end shed), nearly five times that of the dry condition, whereas the 66.7% and 100% fractions yielded peak fields comparable to or lower than the dry case. This behavior stems from the conductivity discontinuity at the wet-dry interface, which concentrates field stress across isolated hydrophilic region, as wetting becomes more continuous, the surface approaches uniform conductivity, allowing more even voltage grading and reduced field enhancement.

Terminal current analysis further showed that the clean and dry condition is purely capacitive, while wetted conditions introduce a resistive leakage component that increases only marginally and monotonically with hydrophilic fraction, showing no correlation with the severe local field enhancement at 22.2% hydrophilicity. This indicates that terminal current monitoring alone cannot reliably detect the localized high-field regions responsible for dry-band arcing. Overall, partial rather than complete hydrophobicity loss is identified as the most critical degradation condition, with the HV end first shed being the most vulnerable to field-induced discharge. These findings highlight the need for field-based localized stress monitoring alongside conventional leakage current measurement for accurate condition assessment of polymer insulators.

Acknowledgement

The author sincerely acknowledges Mr. Hiren M. Patel Assistant Professor and Electrical Engg. Department, FoTE**,** The Maharaja Sayajirao University of Vadodara, India for its continuous academic support and encouragement.

References

[1] C. V. Santoshbhai, A. S. Khopkar, and H. M. Patel, "Comprehensive Comparison of High Voltage Polymer and Porcelain Insulators in AC Systems," Engineering and Technology Journal, vol. 11, no. 01, Jan. 2026, doi: 10.47191/etj/v11i01.38.

[2] C. V. Santoshbhai, A. S. Khopkar, and H. M. Patel, "A Study on Performance of Ageing High Voltage Polymer Insulators in AC Systems," Engineering and Technology Journal, vol. 11, no. 07, Jul. 2026, doi: 10.47191/etj/v11i07.14.

[3] S. M. Gubanski, "Modern outdoor insulation - concerns and challenges," in IEEE Electrical Insulation Magazine, vol. 21, no. 6, pp. 5-11, Nov.-Dec. 2005, doi: 10.1109/MEI.2005.1541483.

[4] B. Venkatesulu and M. J. Thomas, "Corona aging studies on silicone rubber nanocomposites," in *IEEE Transactions on Dielectrics and Electrical Insulation*, vol. 17, no. 2, pp. 625-634, April 2010, doi: 10.1109/TDEI.2010.5448120.

[5] S. Kumagai and N. Yoshimura, "Electrical and environmental stress and the hydrophobic stability of SIR, EVA and their blends," in *IEEE Transactions on Dielectrics and Electrical Insulation*, vol. 8, no. 4, pp. 679-686, Aug. 2001, doi: 10.1109/94.946723.

[6] B. X. Du, H. Xu, and Y. Liu, "Effects of wind condition on hydrophobicity behavior of silicone rubber in corona discharge environment," IEEE Transactions on Dielectrics and Electrical Insulation, vol. 23, no. 1, pp. 385–393, Feb. 2016, doi: 10.1109/TDEI.2015.005463.

[7] R. Chakraborty and S. B. Reddy, "Performance of Silicone Rubber Insulators under Thermal and Electrical Stress," IEEE Trans. Ind. Appl., vol. 53, no. 3, pp. 2446–2454, May 2017, doi: 10.1109/TIA.2017.2672667.

[8] I. Ahmadi-Joneidi, A. Majzoobi, A. Abbas Shayegani-Akmal, H. Mohseni, and J. Jadidian, "212 I. Ahmadi-Joneidi et al.: Aging Evaluation of Silicone Rubber Insulators Using Leakage Current and Flashover Voltage Analysis Aging Evaluation of Silicone Rubber Insulators Using Leakage Current and Flashover Voltage Analysis," 2013.

[9] D. A. Swift, C. Spellman, and A. Haddad, "D.A. Swift et al.: Hydrophobicity Transfer from Silicone Rubber to Adhering Pollutants and its Effect on Insulator Performance Hydrophobicity Transfer from Silicone Rubber to Adhering Pollutants and its Effect on Insulator Performance," 2006.

[10] R. Zeng, Y. Zhang, W. Chen, and B. Zhang, "R. Zeng et al.: Measurement of Electric Field Distribution Along Composite Insulators by Integrated Optical Electric Field Sensor Measurement of Electric Field Distribution Along Composite Insulators by Integrated Optical Electric Field Sensor," 2008.

[11] A. Phillips et al., "Electric fields on AC composite transmission line insulators," IEEE Transactions on Power Delivery, vol. 23, no. 2, pp. 823–830, 2008, doi: 10.1109/TPWRD.2007.911127.

[12] M. M. Hussain, S. Farokhi, S. G. McMeekin and M. Farzaneh, "Effect of uneven wetting on E-field distribution along composite insulators," 2016 IEEE Electrical Insulation Conference (EIC), Montreal, QC, Canada, 2016, pp. 69-72, doi: 10.1109/EIC.2016.7548568.

[13] A. A. Salem et al., "Investigation of High Voltage Polymeric Insulators Performance under Wet Pollution," Polymers (Basel)., vol. 14, no. 6, Mar. 2022, doi: 10.3390/polym14061236.

[14] H. P. Shrimathi, M. Mondal, and P. Mishra, "Simulation based electric stress estimation on silicone rubber polymeric insulators under multi-environmental conditions," Electric Power Systems Research, vol. 214, Jan. 2023, doi: 10.1016/j.epsr.2022.108840.

[15] M. Batalović, H. Matoruga, S. Berberovic, M. Matoruga, and S. Berberović, "Influence of Environmental Stresses on High Voltage Polymer Rod Type Insulator Performances." [Online]. Available: https://www.researchgate.net/publication/328734120

[16] M. Asif, K. Al-Soufi, U. A. Khan, and L. M. Alhems, "Intensification of Electric Field Stresses in Field Aged 380-kV Composite Insulators Due to Loss of Hydrophobicity," IEEE Access, vol. 12, pp. 38849–38866, 2024, doi: 10.1109/ACCESS.2024.3375399.

[17] X. Yu, Q. Zhang, X. Yang, H. Yang, J. Zhou, and B. Liu, "Influence of non-uniform hydrophobicity distribution on pollution flashover characteristics of composite insulators," IET Science, Measurement and Technology, vol. 12, no. 8, pp. 1009–1014, Nov. 2018, doi: 10.1049/iet-smt.2018.5266.

[18] Vrushank S. Chavan, Hiren M. Patel, Dr. Anil S. Khopkar, "Electric Stress Analysis of Ageing 400 KV Composite Insulator Profiles Having Internal Defects," *International Journal of Emerging Trends in Engineering Research*, vol. 14, no. 6, pp. 103–110, Jun. 2026, doi: 10.30534/ijeter/2026/0114062026.

[19] H. P. Shrimathi, M. Mondal, and P. Mishra, "Simulation based electric stress estimation on silicone rubber polymeric insulators under multi-environmental conditions," Electric Power Systems Research, vol. 214, Jan. 2023, doi: 10.1016/j.epsr.2022.108840

Author Profile

Mr. Chavan Vrushank Santoshbhai completed his B.E. in Electrical Engineering from Gujarat Technological University, India. He is currently pursuing M.E. in Electrical Power Engineering at The Maharaja Sayajirao University of Baroda, India. He is undertaking his postgraduate project under the expert guidance of Electrical Engg. Department, FoTE, The Maharaja Sayajirao University of Vadodara, India. His research area focuses on high-voltage polymer insulator performance, and his interests include finite element analysis of electrical equipment and power system studies. He can be contacted at email: vrushank.msu@gmail.com